(Engineering Note)

Numerical Study of Flow and Heat Transfer in a Pre-swirl System

M. Farzane-Gord[1]
Dep't. Mech. Eng.
Shahrood Univ. of Tech.

ABSTRACT

Pre-swirl is often used in the internal cooling-air systems of gas turbines to reduce the temperature of the cooling air relative to the rotating turbine blades. In a "direct-transfer" system, the air passes axially across the wheel-space from stationary pre-swirl nozzles to receiver holes in the rotating turbine disc. This paper investigates the effects of inlet flow conditions and rotational speed on the flow and the heat transfer in such system, using a simplified computational model for three-dimensional steady, incompressible turbulent flow based on an in-house solver developed by the author. The computed results are compared with measurements of tangential velocity and Nusselt number and show that there are significant mixing losses near the inlet nozzles, resulting in a reduced "effective" pre-swirl ratio at inlet. The computed tangential velocity distributions suggest free-vortex-type behaviour for the flow between the pre-swirl nozzle radius and that of the receiver holes. There is mainly good agreements between the computed and the measured velocities, although the measured values are generally lower than the computed ones and follow free-vortex behaviour less closely. There is less agreements between the computed and the measured values of Nusselt number, although the correct trends are obtained for the effects of the main flow parameters.

Key Words: Gas Turbine, Cooling Systems, Pre-swirl Rotor-Stator System, Direct Transfer Pre-swirl System

مطالعه عددی جریان سیال و انتقال حرارت در یک محفظه پیش-چرخش

محمود فرزانه گرد
دانشکده مهندسی مکانیک، دانشگاه صنعتی شاهرود
(تاریخ دریافت: ۱۳۸۵/۳/۲۳؛ تاریخ پذیرش: ۱۳۸۷/۱/۲۶)

چکیده

پیش چرخش اغلب در سیستم‌های خنک‌کاری داخلی توربین‌های گازی برای کاهش دمای نسبی هوای خنک کننده نسبت به پره‌های چرخنده توربین استفاده می‌شود. در سیستم "انتقال مستقیم" هوا فاصله محوری بین نازل‌های پیش- چرخش روی دیسک ثابت و حفره‌های هوای خنک‌کن پره‌ها قرار گرفته روی دیسک چرخان را به طور مستقیم طی می‌کند. در این مقاله، اثر شرایط جریان ورودی و سرعت دورانی روی جریان سیال و انتقال حرارت درون چنین محفظه‌ای بررسی شده است. در این بررسی، از یک مدل ساده شده عددی برای جریان تراکم ناپذیر و پایدار آشفته استفاده شده است. مدل ذکر شده بر پایه یک برنامه رایانه‌ای توسعه داده شده توسط نویسنده است. نتایج عددی حاصل برای سرعت مماسی و عدد ناسلت با نتایج آزمایشگاهی مقایسه شده‌اند. نتایج عددی نشان دهنده اتلافی چشم‌گیر در اثر اختلاط در ورودی است. این اتلاف باعث کاهش ضریب پیش-چرخش مؤثر در ورودی می‌شود. تغییرات مقادیر عددی سرعت مماسی بین شعاع ورودی وخروجی نشان رفتار جریان ورتکس آزاد است. معمولاً مقادیر تجربی و عددی مؤلفه‌های سرعت هم‌خوانی خوبی را نشان می‌دهند. در ضمن، مقادیر تجربی رفتار جریان ورتکس آزاد را با شدت کمتری نشان می‌دهند. همچنین، مقادیر تجربی و عددی برای عدد ناسلت هم‌خوانی کمتری را نشان می‌دهند، هر چند نتایج عددی و تجربی رفتار یکسانی را در اثر تغییرات ضرایب مؤثر جریان نشان می‌دهند.

کلید واژه‌ها: توربین‌های گازی، سیستم خنک‌کاری، سیتم‌های پیش-چرخش روتور و استاتور، سیتم‌های پیش-چرخش انتقال مستقیم

1-Assistant Professor: mgord@shahroodut.ac..ir

I. NOMENCLATURE

a , b	Inner, Outer Radius of Disc
c_p	Specific Heat of Air at Constant Pressure
C_p	Static Pressure Coefficient $(=2(P_\infty - P_p)/ \Omega r_p^2)$
C_w	Non-dimensional Mass Fow Rate $(= \dot{m} /\mu b)$
$C_{o,p}$	Total Pressure Coefficient $(=2(P_{o,\infty} - P_{o,p})/ \Omega r_p^2)$
d	Pre-swirl Nozzle Diameter
G	Gap ratio (= s/b)
k	Turbulence Kinetic Energy, Thermal Conductivity of Air
$\dot{m}$	Mass Flow Rate
N	Number of Pre-swirl Nozzles (or Balde Cooling Holes)
Nu	Local Nusselt Number $(=qr/k(T_{aw} - T_w))$
P, P_o	Static and Total Pressure
Pr	Prandtl Number $(=\mu c_p /k)$
q	Heat Flux (from Air to Disc)
r, ϕ, z	Radial, Tangential and Axial Coordinates
R	Recovery Factory $(=Pr^{1/3})$
Re_ϕ	Rotational Reynolds Number
s	Axial Spacing Between Stator ($z=0$) and Rotor ($z=s$)
T	Temperature
T_a	Total Temperature of Pre-swirl Air at Inlet
T_w	Temperature at Rotor Disc Surface (Wall)
U_τ	Friction Velocity $(=\sqrt{\tau_w / \rho})$
V_r, V_ϕ, V_z	Time-averaged Radial, Circumferential, Axial Components of Velocity
x	Non-dimensional Radius (= r/b)
y	Distance Normal to the Wall
y+	Non-dimensional Distance $(= \rho y U_\tau/\mu)$
z	Axial Distance
β	Swirl Ratio $(= V_\phi /\Omega r)$
β_p	Pre-swirl Ratio $(= V_{\phi,p} /\Omega r_p)$
ε	Turbulence Energy Dissipation Rate
λ_T	Turbulent Flow Parameter $(= C_{w,p}/Re_\phi^{0.8})$
θ	Angle of Pre-swirl Nozzle to Tangential Direction
μ	Dynamic Viscosity
ρ	Density
τ_w	Wall Shear Stress
Ω	Angular Speed of Disc

Subscripts

aw	Adiabatic Wall Value
b	Blade-cooling Air, at Receiver Hole radius
p	Pre-swirl Air, at Pre-swirl Nozzle Radius
s	Sealing Air
∞	Mid-plane $z/s=0.5$ (Outside of Boundary Layers)

INTRODUCTION

Figure **1** shows the flow of the cooling air due to confined discs of typical internal-air system used in gas-turbines. The exit of the compressor is the source for the turbine blade-cooling air. To increase the efficiency by increasing the compressor pressure ratio in turn increases the temperature of the cooling air, which makes cooling more difficult. The temperature of the air entering the blade-cooling holes can be reduced in the rotating system by swirling the cooling air in the direction of the turbine disc. Such systems are called pre-swirl cooling systems.

As shown in Fig.1, the geometries in real engines are very complicated. In order to understand the flow and heat transfer over these complicated surfaces, it is usual to simulate the geometries by plane rotating-disc systems. A turbine disc usually rotates next to either a stationary or another rotating disc, and these can be simulated by the rotor-stator, rotating cavity or contra-rotating disc systems.

A rotor-stator system, as shown in Fig. 2, provides a simplified model for the flow and heat transfer that occurs in the wheel-space between an air-cooled turbine disc and adjacent stationary casing. It is known as "direct-transfer" pre-swirl system that is used in some engines. The pre-swirl nozzles are located at a low radius on the stator and the cooling air flows radially outward to the receiver holes through the rotating cavity between the stationary disc and rotating disc.

Enim et al. [1] studied "direct transfer" pre swirl systems using the commercial multi-purpose CFD code Fluent. The computations were carried out using a steady-state 3D method and a so-called “frozen rotor” approach for treating the interface between the stationary and rotating domains.

Geis et al. [2] measured the cooling efficiency of a pre-swirl rotor-stator system equipped with a small number of pre-swirl nozzles of circular shape, located on a radius equal to that of the receiver holes. They compared their experimental data with a simple theoretical model, which predicted air temperatures in an "ideal" pre-swirl system. It was found that the pre-swirl system performed worse, in terms of cooling air temperature reduction, than was expected for isentropic flow.

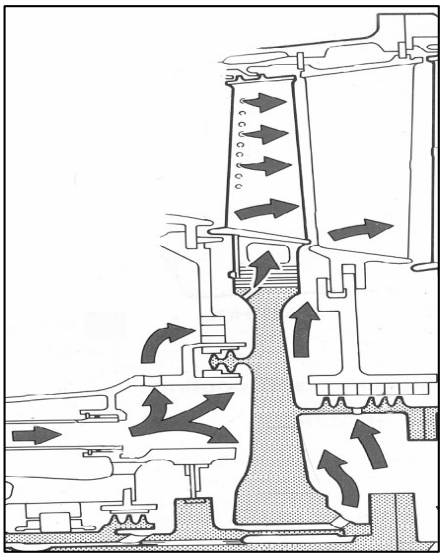

Fig. (1): Typical turbine cooling (From "The Jet Engine" Rolls-Royce PLC [9]).

The flow and heat transfer in a "direct-transfer" pre-swirl model of pre-swirl rotor-stator system in which pre-swirl nozzles and blade cooling holes were located in same radius were studied by Wilson et al [3], who found that the pre-swirl flow mixed fully with a superposed radial outflow of disc-cooling air before entering the receiver holes. Greater losses in total pressure are expected for direct transfer system compared with the free-vortex flow found in other arrangement of rotor-stator system, known as cover plate, due to strong mixing between the pre-swirl flow and the re-circulating rotor-stator flow in the chamber.

Yan et al. [4] carried out measurements and three dimensional computations for the flow structure in an idealised pre-swirl rotor-stator system, and Farzaneh et al. [5] described an investigation of the heat transfer in the same system where blade cooling holes modeled as a ring. The results obtained show that the flow in the pre-swirl system has some similarities with that found in classical rotor-stator systems. The measurements and computations showed that significant losses in total pressure occurred between the inlet nozzles and the mid-axial plane between the rotor and stator (where pitot-tube measurements were made). These mixing losses, which were caused by a momentum exchange between the primary pre-swirl flow and the recirculating secondary flow, increased as the inlet pre-swirl ratio increased.

Karabay [6] carried out a combined experimental and computational study of flow in a "cover-plate" pre-swirl system. The cooling air from the stationary pre-swirl nozzles flowed radially outward (to the receiver holes) in a rotating cavity formed by the rotating disc and a cover-plate attached to it. Free vortex flow was found to occur for this system, and a theoretical analysis was used to show that there was an optimal value of the pre-swirl ratio, for which the average Nusselt number for a heated rotating disc would be a minimum.

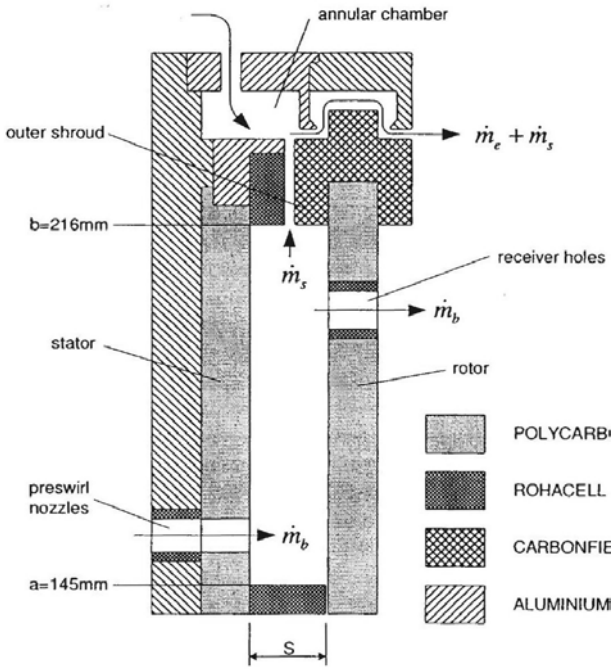

Fig. (2): Schematic diagram of experimental pre-swirl rig (Yan et al. [4], not to scale).

Mirzaee et al. [7] presented the heat transfer in a rotating cavity with a stationary outer shroud for the case of a peripheral inflow and outflow of cooling air. They also included the effect of the radiation heat transfer on computed local Nusselt numbers. The radiation heat transfer was calculated between measured temperatures on the heated disc and computed surface temperatures on the other unheated surfaces. They applied a conductive-disc assumption for the unheated-disc thermal boundary condition, which improved the agreement of Nusselt numbers significantly between computations and measurements for the heated disc. Based on the same computation model and solver, Mirzaee [8], showed reasonable agreement with measurement for heat transfer computations in a rotating cavity with a stationary stepped-shroud system.

Earlier research into direct transfer systems, and rotor-stator systems in general, was described by Owen and Rogers [9] and Owen and Wilson [10] gave a brief review of more recent heat transfer research.

This paper studies the effects of blade cooling holes on heat transfer coefficients over rotating disc

surfaces. As three dimensional steady code has been developed in rotating frame of references to model blade cooling holes, pre-swirl nozzles were needed to be modeled as an annular ring. This allows computing local heat transfer coefficients around the blade cooling holes which suspected to be high. For validating the numerical method, the measured data and computed values of [4] and [5] are also compared with computation values.

In this paper based on a three dimensional steady state solver developed by Author, the steady flow model used by Yan et al. [4] has been extended to make corresponding heat transfer predictions, and the further details of the model are given below. Computed and measured tangential velocity distributions are used to investigate free-vortex type behaviour in the system and the mixing losses near the pre-swirl inlets. Computed and measured distributions of Nu over the disc surface are presented, and the variation of Nu with λ_T and Re_ϕ is described for both the measured data [5] and the computed results. The paper also studies the effects of blade cooling holes on heat transfer coefficients over rotating disc surfaces. As the three dimensional steady code has been used in rotating frame of references to model blade cooling holes, pre-swirl nozzles were needed to be modeled as an annular ring. This allows computing local heat transfer coefficients around the blade cooling holes which suspected to be high.

GOVERNING EQUATIONS

The three dimensional, steady state, incompressible Reynolds-averaged flow equations in a cylindrical polar coordinate system r, Φ ,z with velocity components V_r, V_Φ, V_z can be written as common form in fixed and rotating frame of reference:

$$\frac{1}{r}\frac{\partial}{\partial r}\left(\rho r V_r \Phi\right)+\frac{1}{r}\frac{\partial}{\partial \phi}\left(\rho V_\phi \Phi\right)+\frac{\partial}{\partial z}\left(\rho V_z \Phi\right) = \frac{1}{r}\frac{\partial}{\partial r}\left(r\Gamma_r \frac{\partial \Phi}{\partial r}\right)+\frac{1}{r^2}\frac{\partial}{\partial \phi}\left(\Gamma_\phi \frac{\partial \Phi}{\partial \phi}\right)+\frac{\partial}{\partial z}\left(\Gamma_z \frac{\partial \Phi}{\partial z}\right)+S_\Phi \ , \quad (1)$$

where, Φ represents the generalised momentum variable and the net source S_Φ is different for each component of momentum. Γ_r, Γ_Φ , and Γ_z are the effective diffusivities for the radial, circumferential and axial directions comprising both laminar and turbulent components. The relevant expressions are summarized in Table (1), in which $\mu_{eff}=\mu+\mu_t$ is the effective viscosity.

It should be pointed out that in rotating frame of references, underlined terms are vanished and in the momentum equations, P which denotes reduced pressure, is calculated as below where P_s is pressure in stationary frame of references:

$$P = P_s - \rho r^2 \Omega^2 \quad . \quad (2)$$

In this paper, turbulent flow computations have been made using the low-Reynolds number k-ε turbulence model proposed by Launder-Sharma [11] with turbulent heat transfer represented using a turbulent Prandtl number, Pr_t, equal to 0.9.
The k-ε turbulence model equations can be represented in the same common form of equation **1**. In the k-ε equations, P_e denotes the rate of production of turbulent kinetic energy and is given as follows:

$$P_e = \mu_t \left[\begin{array}{l} 2\left(\left(\frac{\partial V_z}{\partial z}\right)^2+\left(\frac{\partial V_\phi}{r\partial \phi}+\frac{V_r}{r}\right)^2+\left(\frac{\partial V_r}{\partial r}\right)^2\right)+ \\ \left(\frac{\partial V_z}{\partial r}+\frac{\partial V_r}{\partial z}\right)^2+\left(\frac{\partial V_\phi}{\partial z}+\frac{V_z}{r\partial \phi}\right)^2+ \\ \left(r\frac{\partial}{\partial r}\left(\frac{V_\phi}{r}\right)+\frac{\partial V_r}{r\partial \phi}\right)^2 \end{array} \right] . \quad (3)$$

Other terms appearing in the k-ε equations are given in Table 2. f_μ is a wall damping function associated with low Reynolds number models. R_t is a local turbulence Reynolds number and y^+ is the non dimensional distance from the solid surface:

$$R_t = \frac{\rho \kappa^2}{\mu \varepsilon} \ , \quad (4)$$

and

$$y^+ = y_{\min}\sqrt{\frac{\tau_w}{\rho}} / \nu \quad . \quad (5)$$

In equation (5), y_{min} is taken as the minimum distance between the wall and the mesh point and τ_w is the average wall shear stress.

Yap empirical correction, YC, is added to source term of ε equation intending to reduce unrealistically large levels of near-wall turbulence that are returned by the Launder-Sharma model in regions of flow separation. Craft et al. [15] showed that the unrealistic large peak in Nusselt number prediction for impinging flows can be improved with the use of the Yap correction term as:

$$YC = \max\left[0.83\left(\frac{l}{l_\theta}-1\right)\left(\frac{l}{l_\theta}\right)\frac{2\varepsilon^2}{k}, 0\right] , \quad (6)$$

where,

$$l_\theta = k^{1.5} / \varepsilon \quad , \qquad (7)$$

and $l=2.55y$ which y is the normal wall distance.

COMPUTATIONAL PROCEDURE

The governing equation were discretised using a finite-volume method with hybrid-differencing for convection terms. The SIMPLE approach is adopted within staggered grid arrangement, and the algebraic equations were solved using a tri-diagonal matrix algorithm (TDMA) iteratively in an ADI fashion. A Gosman [12] type damping function, *GSF*, was used as fallows to improve convergence for radial momentum equation:

$$GSF = \alpha_G \frac{\rho |V_\phi|}{r} (V_r^{old} - V_r^{new}) \qquad (8)$$

Where, α_G is empirical constant.

GEOMETRY AND GRID DISTRIBUTION

A schematic diagram of the geometry modeled is shown in Fig. 2. It is based on an experimental rig of [4] shown in Fig 2 in which there were 24 pre-swirl nozzles, angled at 20^o to the tangential direction, in the stator, and 60 axial receiver holes in the rotor. The radial location of the nozzles, for which $x_p=r_p/b=0.74$, was less than the centerline radius of the blade cooling holes at $x_b=r_b/b=0.93$.

The three dimensional steady incompressible flow model involves one of the discrete pre-swirl nozzles on the stator in stationary frame of reference with cyclic symmetry conditions applied at the tangential faces of the domain. In order to permit steady flow computations, an annular outlet is used on the rotor. This outlet matches the centerline radius and total flow area of the sixty receiver holes. To study heat transfer coefficients around bald-cooling holes, inlet nozzles modeled as annular inlet and blade cooling holes as discrete hole on rotor in rotating frame of references.

Due to satisfy the Low-Reynolds $\kappa-\varepsilon$ model requirements ($y^+ < 0.5$), a large number grid points was packed near wall and to model the inlet and outlet, fine grid used in these area as tried to keep the expansion/contraction parameter lower than *1.2*, The grid distribution tests showed that a *140×297×12* grid points (axial x radial x tangential) was required in rotating frame and *140×211×40* in stationary frame. The meshes are illustrated in Fig. 3a and Fig. 3b respectively.

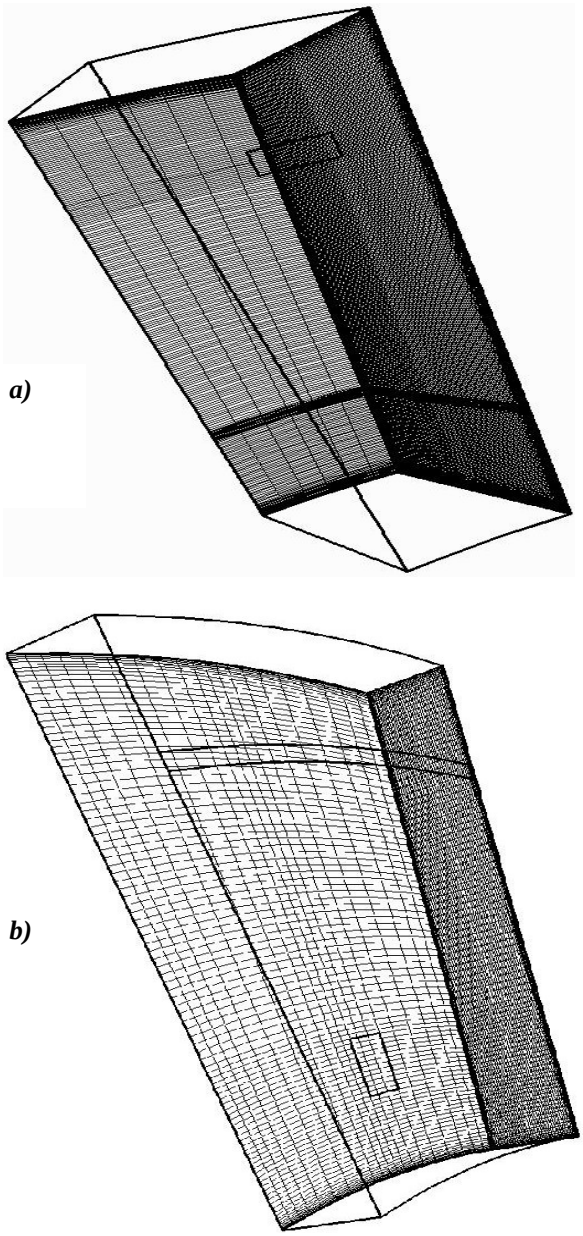

Fig. (3): The grid distribution used in computation (every 2&3 points are shown)
a) rotating frame (140×297×12)
b) stationary frame(140×211×40).

BOUNDARY CONDITION

No-slip boundary condition was used for the velocity components on the solid surface. The uniform axial velocity was used from the specified mass flow rate and tangential velocity component was set up to have an angled flow at inlet. At the outlet, the uniform axial velocity was used to ensure continuity, and tangential velocities were computed from a zero normal derivative condition. The radial velocity component was set to zero at inlet and outlet.

For heat transfer computation, adiabatic thermal boundary conditions were used for solid surfaces other than for the rotating disc for which kept constant at 20° C except in a case when the effects of disc temperature were investigated. The inlet flow total temperature was kept constant at 55° C, and a zero normal-derivative condition was used for the outlet. Fluid properties were calculated at 20° C, as in the experiments [4].

In this paper, cyclic boundary conditions were applied in tangential direction. For *N* blade cooling holes (or *N* pre-swirl nozzles in case of stationary frame), this enable modeling only $360^o/N$ angular sector to represent the whole system.

RANGE OF FLOW PARAMETERS

According to [10] the most effective dimensionless parameters that control flow inside a rotor-stator system are inlet swirl ratio, β_p, non-dimensional mass flow rate, C_w, rotational Reynolds number, Re_ϕ, and turbulent flow parameter, λ_T. It is also shown by [6] that rotational Reynolds number is less effective parameter in cover plate pre-swirl arrangement. Yan et al. [4] are also concluded that the flow structure in the pre-swirl chamber is controlled principally by the pre-swirl ratio and the turbulent flow parameter.

The parameter ranges covered numerically are same as in [4] & [5] were as follows:

$$0.78 \times 10^6 < Re_\phi < 1.2 \times 10^6,$$
$$0.6 \times 10^4 < C_w < 2.8 \times 10^4 \ (0.11 < \lambda_T < 0.36)$$
$$0.5 < \beta_p < 3.0 \quad .$$

The ranges of λ_T and β_p are typical of those used in practice. Whilst the maximum Re_ϕ value of is an order of magnitude smaller than that found in engines, the flow structures and trends in heat transfer described here are believed to be representative.

RESULTS & DISCUSSTION

Effect of frame of references

To study the effect of frame of references, computed value of static and total pressure coefficients are compared along with the measured value of [4]. The pressure coefficients are computed as described in [4].

Figures **4a** and **4b** show radial variation of static and total pressure coefficients in mid r-z plane. As it can be seen the computed result for stationary frame shows better agreement with measured values.

As shown above, computed results in stationary frame of references give better agreement with measured values compared with computed results in rotating frame of references this is mainly because of modeling inlet as in stationary frame a discrete nozzle and in rotating frame an annular ring were used. This shows significant effects on computed values. It also should be pointed out that inlet modeling in stationary frame is closer to experiments of [4].

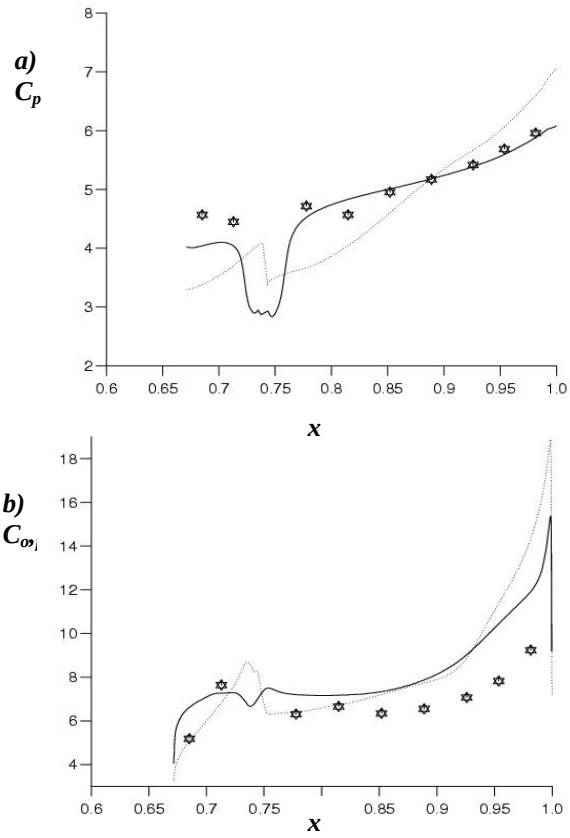

Fig (4): Computed and measured distribution of pressure coefficients (mid r-z plane)
…. Computed (rotating frame)
─ Computed (stationary frame)
⎔ measured [4].

Figure **5** shows distributions of computed local heat transfer coefficients over the rotating disc surface, As it can be seen, it shows nearly axisymmetric behaviour except in the regions around and between blade cooling holes. The same result are also obtained by Lock et al. [13] using liquid crystal measurement. Their results were also shown generally good repeatability of heat transfer coefficients obtained between different pairs of holes.

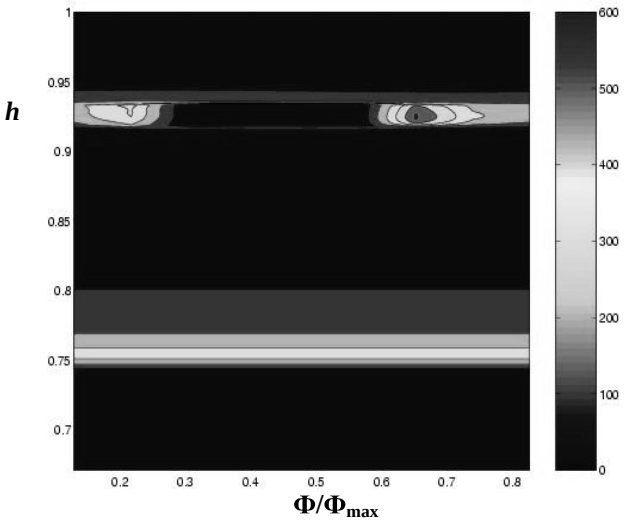

Fig 5: Computed distribution of local heat transfer coefficient over rotating disk (w/m^2 k) (rotating frame)**.**

The heat transfer results showed nearly axisymmetric behaviour and computed value in stationary frame of references have better agreement with measured value so rest of the result are computed in stationary frame of references.

Swirl ratio and effective pre-swirl ratio

Yan et al. [4] showed comparisons between computed and measured variations of (tangentially-averaged) swirl ratio β_∞ ($=V_{\phi,\infty}/\Omega r$) with non-dimensional radius x (=r/b) along the mid-plane between the rotor and stator (z/s=0.5). Figures **3** and **4** show further comparisons, for a range of test conditions, plotted against x^{-2} instead of against x. The technique of plotting β_∞ against x^{-2}, which was used by Karabay et al. [6], is described below.

Under ideal conditions, the air from the pre-swirl nozzles would flow radially outward creating a free vortex, where:

$$\beta_\infty = \beta_p \left(\frac{x_P}{x} \right)^2 . \qquad (9)$$

For this system, the free vortex defined by Eq. (9) will have a value of $\beta_\infty = \beta_p$ at $x^{-2} = 1.826$.

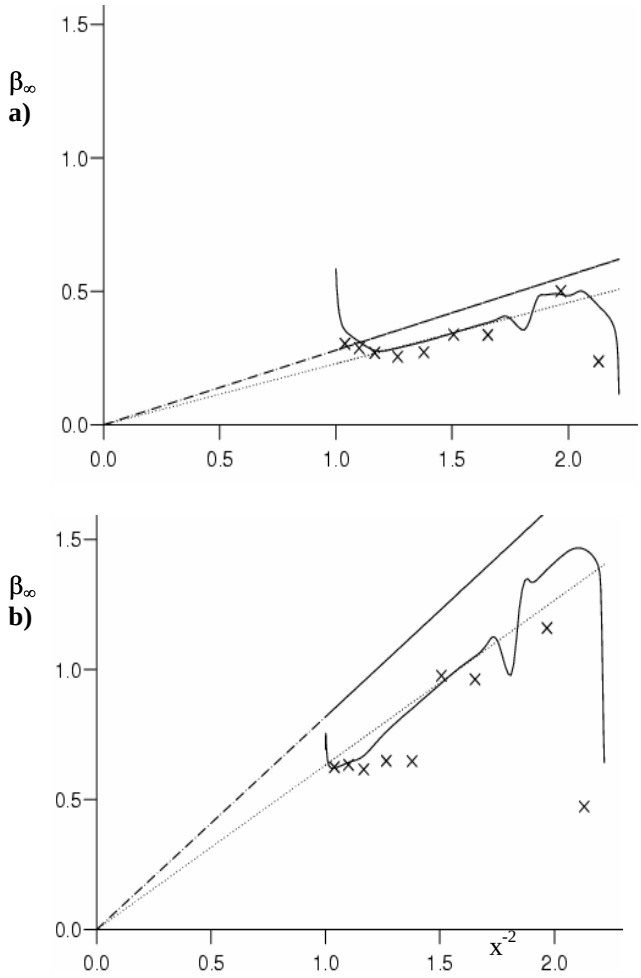

Fig. 6: Computed and measured radial variation of β_∞
a) $Re_\phi = 0.80\times10^6$, $\lambda_T = 0.126$, $\beta_p = 0.51$
b) $Re_\phi = 0.78\times10^6$, $\lambda_T = 0.369$, $\beta_p = 1.49$
——— computed, × measured,
- - - - - ideal free vortex, Eq. (9),
..... effective free vortex, Eq. (10).

This "ideal" free vortex is shown, as a straight line passing through the origin, in Fig's. **6** and **7**. In fact, *any* straight line passing through the origin in these plots correspond a free vortex. Due to the momentum losses that occur as the pre-swirl flow mixes with the recirculating flow, the gradient of the actual free vortex will be less than that of the ideal free vortex. It is convenient, therefore, to define an *effective* pre-swirl ratio, $\beta_{p,eff}$, to represent the actual free-vortex flow, such that:

$$\beta_\infty = \beta_{p,eff} \left(\frac{x_P}{x} \right)^2 , \qquad (10)$$

where, $\beta_{p,eff} < \beta_p$. This "effective free-vortex", based on Eq. (10), is also shown in Figs. 6 and 7. The value of $\beta_{p,eff}$ has been taken as the computed value of β_∞ at $x^{-2} = 1.826$ (where $x = x_p$).

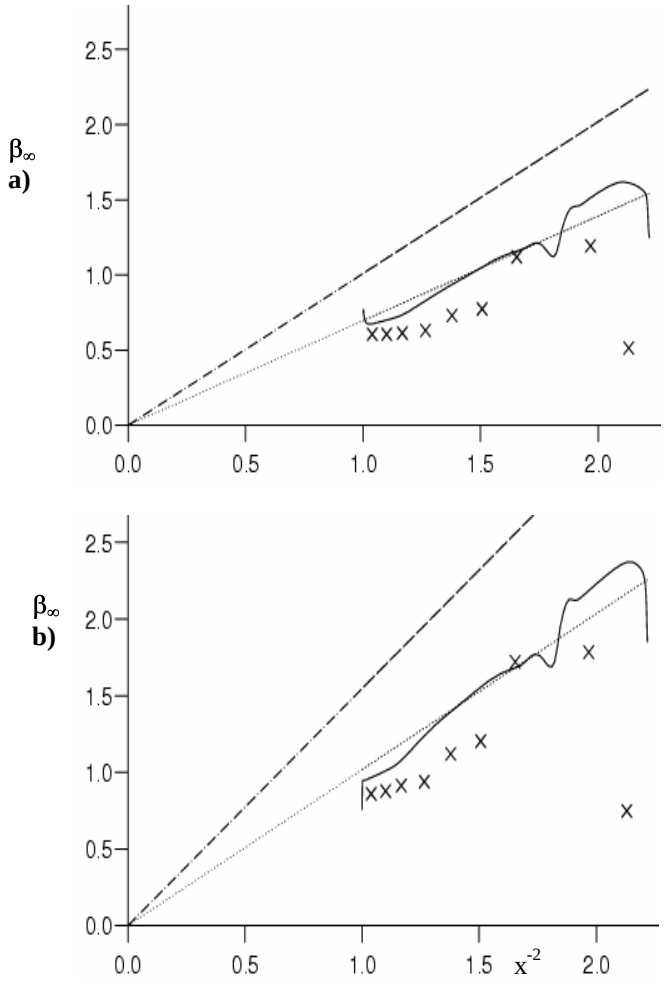

Fig. (7): Computed and measured radial variation of β_∞ (for legend see Fig. 6)
a) $Re_\phi = 1.18\times10^6$, $\lambda_T = 0.245$, $\beta_p = 1.84$
b) $Re_\phi = 0.79\times10^6$, $\lambda_T = 0.347$, $\beta_p = 2.82$

Fig. **6** and Fig. **7** show that the computed distributions of β_∞ follow free vortex behaviour quite closely between the pre-swirl nozzle radius and the receiver outlet radius, $x = x_b$. The computed results shown in Fig. **6** are in reasonably good agreement with the measurements, although the measured values are generally lower than the computed values, suggesting higher mixing losses in the experiments and hence a lower value for $\beta_{p,eff}$. The same comments apply for the results shown in Fig. **7**, however there is less good agreement between the computations and measurements for these higher β_p cases. The difference between $\beta_{p,eff}$ and β_p increases as β_p increases. Fig. **8** shows that the computed variation is represented reasonably well by the following correlation:

$$\frac{\beta_{p,eff}}{\beta_p} = 0.700 - 0.065\beta_p \quad . \tag{11}$$

Karabay et al. [6] also found that a correlation of this form (with different coefficients) described the variation of $\beta_{p,eff}$ with β_p in a simplified cover-plate (rotating cavity) system as described above.

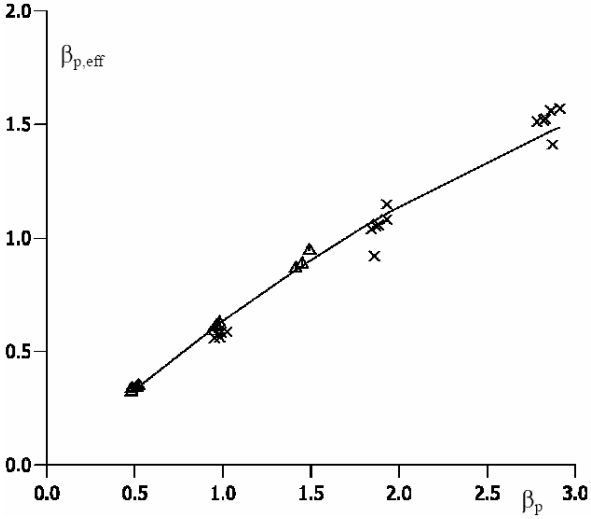

Fig. (8): Computed variation of $\beta_{p,eff}$ with β_p
Δ , $\times$ measured [4] , _____ Eq. (11)

Radial variation of local Nusselt number
The local Nusselt number, Nu, is defined as:

$$Nu = \frac{qr}{k(T_w - T_{aw})} \quad , \tag{12}$$

where,:

$$T_{aw} = T_a + \frac{1}{2c_p}\left\{R(\Omega r - V_{\phi,\infty})^2 - V_{\phi,\infty}^2\right\} . \tag{13}$$

Equation (13) for T_{aw} is based on the theoretical adiabatic-wall temperature given by Karabay et al. [6], although making use of the measured total temperature of the inlet air, T_a. The transient heat transfer experiments give rise to a time-varying distribution of temperature T_{aw} over the unheated

rotor; for the steady-state computations, the initial air temperature measured prior to the start of each transient test was used as the uniform disc temperature. (Studies suggest that computed Nu is not sensitive to the radial variations of temperature that occur with time in the experiments.) Temperatures on the stator, and on the inner and outer surfaces, were not measured in the experiments and adiabatic conditions were assumed for the computations.

Figure **9** shows the effect of Re_ϕ on the computed and measured radial variation of Nusselt number at two fixed values of λ_T (0.125 and 0.36 approx.), for which $\beta_P \approx 0.5$ and 1.4, respectively. The measurements correspond to a radial line lying mid-way between receiver holes obtained by Lock et al. [13]. For the computational model an annular receiver outlet is used (see Fig. **3b**), and comparisons with measurements made in the region between holes cannot be made.

For both fixed values of λ_T (and of β_P) shown in Fig. **9**, the magnitude of Nu increases with increasing Re_ϕ, but there is little effect of Re_ϕ on the shape of the Nu distributions (for either the computations or the measurements). For all cases, there is a local peak in measured values of Nu in the region near the receiver holes on the disc. Both the measured and the computed results are discussed below.

Referring to the measurements, Fig. **9a** ($\lambda_T \approx 0.125$, $\beta_P \approx 0.5$) shows that Nu increases with radius between the pre-swirl nozzle radius, $x_p = 0.74$, and the receiver holes. These results suggest that the heat transfer is controlled mainly by the boundary layer flow on the rotating disc. For $x > 0.9$, there is a rapid rise in measured Nu. In this region, disc boundary layer fluid enters the receiver holes and there is strong flow axially toward the disc, causing an increase in heat transfer.

The computed results for the two $\lambda_T \approx 0.125$, $\beta_P \approx 0.5$ cases shown in Fig. **9a** show a large peak in Nu around the pre-swirl nozzle radius, $x_p = 0.74$. This peak results from the use of a low-Reynolds-number, isotropic k-ε turbulence model in a region where anisotropic impinging-flow effects occur near the rotating disc surface (due to the axial component of the pre-swirl flow). Pilbrow et al [14] found similar behaviour for a different pre-swirl system, and tested an alternative to the Launder-Sharma low-Reynolds-number model used here that gave, in general, a lower peak in the corresponding impingement region. In the present work, there was little difference in results obtained using this alternative model and the Launder-Sharma model.

The computations shown in Fig. **9a** mainly underestimate the measured Nusselt numbers for $x_p < x < x_b$, but the computed increase of Nu with increasing Re_ϕ is in reasonable agreement with the measured trend. Modeling simplifications used at the receiver outlet (as described above) may contribute to the large peaks in computed Nu around $x = 0.93$. Further radially outward, the agreement between computations and measurements is similar to that inward of the receiver holes.

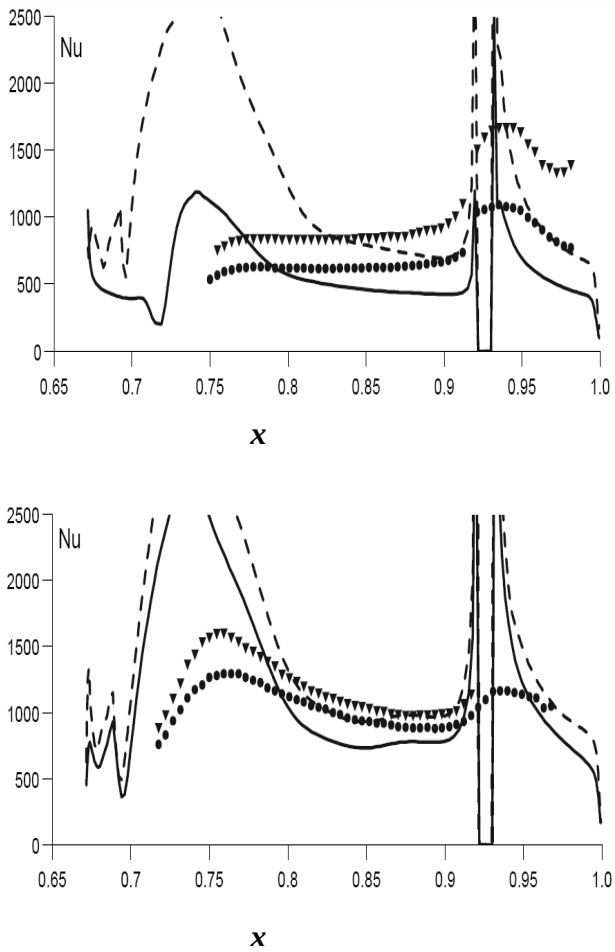

Fig. 9: Effect of Re_ϕ on radial variation of Nu., N= 24
a) $\lambda_T \approx 0.125$, $\beta_p \approx 0.52$; b) $\lambda_T \approx 0.36$, $\beta_p \approx 1.4$
$Re_\phi \approx 0.8 \times 10^6$ ♡ measured , - - - - - computed
$Re_\phi \approx 1.2 \times 10^6$ ▼ measured , ——— computed

Fig. **9b** shows that, for $\lambda_T \approx 0.36$ ($\beta_P \approx 1.4$), a local peak in measured Nu occurs around the inlet nozzle radius x_p, and Nu decreases for $x_p < x < x_b$. This suggests that inertial "impingement" effects, due to the more powerful pre-swirl flow at this higher value of λ_T, have a more significant influence than for the cases shown in Fig. **9a**. Fig. **9b** shows that computations again reproduce the measured trends reasonably well, although the peak in Nu near $x = x_p$ is greatly exaggerated. There is generally better

agreement between the computations and the measurements for the cases shown in Fig. 9b than for those at the lower value of λ_T.

CONCLUSIONS

A computational study has been carried out to investigate the effects of flow rate, swirl ratio and rotational Reynolds number on the flow and heat transfer in a pre-swirl rotating-disc system, representative of that found in gas-turbine cooling systems. Measurements of swirl ratio β_∞, and of local Nusselt number, Nu, on the rotating disc, have been compared with turbulent flow results obtained using a simplified three dimensional steady computational model of the system.

Computations of β_∞ show that the flow structure follows closely free vortex behaviour for $x_p < x < x_b$. Due to mixing losses that occur between the primary pre-swirl flow and the recirculating secondary flow, this free vortex behaviour corresponds to an effective pre-swirl ratio, $\beta_{P,eff}$, which is lower than the inlet pre-swirl ratio β_P. The difference between $\beta_{P,eff}$ and β_P increases as β_P increases. Measured values of β_∞ were found to be lower than computed values.

Measurements and computations of heat transfer both show that values of Nu increase as Re_ϕ, λ_T and β_P increase. The computation suggest that heat transfer is controlled by viscous effects at low values of λ_T, and by inertial effects at high values of λ_T. Measured values of Nu were mainly underpredicted, except in the region around the pre-swirl nozzle radius where inertial "impingement" effects are predicted poorly by the low-Reynolds-number k-ε turbulence model used.

REFERENCES

1. Benim, A.C., Brillert, D., and Cagan M., "Investigation into the Computational Analysis of Direct-transfer Pre-swirl Systems for Gas Turbine Cooling", ASME paper, GT2004-54151, 2004
2. Geis, T., Dittmann M. and Dullenkopf, K., "Cooling Air Temperature Reduction in a Direct Transfer Preswirl System", ASME paper GT2003-38231, 2003
3. Wilson, M., Pilbrow, R., and Owen, J.M., "Flow and Heat Transfer in a Pre-swirl Rotor-Stator System", J. Turbomachinery, Vol. 119, No. 2, pp. 364-373, 1997
4. Yan, Y., Farzaneh-Gord, M., Lock, G.D., Wilson, M.and Owen, J.M., "Fluid Dynamics of a Pre-swirl Rotor-stator System", J. Turbomachinery, Vol. 125, No.1, pp. 641-647, 2003
5. Farzaneh-Gord, M., Wilson, M., and Owen, J.M., "Effects of Swirl and Flow Rate on the Flow and Heat Transfer in a Pre-swirl Rotating-disc System", Int. Gas Turbine Congress, Tokyo, paper, TS-064, 2003
6. Karabay, H., Wilson, M. and Owen, J.M., "Predictions of Effect of Swirl on Flow and Heat Transfer in a Rotating Cavity", Int. J. Heat Fluid Flow, Vol. 22, No. 1, pp 143-155, 2001
7. Mirzaee, I., "Computation of Flow and Heat Transfer in a Rotating Cavity with Peripheral Flow", PhD thesis, Univ. of Bath, UK, 1997
8. Mirzaee, I., Gan, X., Wilson, M., and Owen, J.M. "Heat Transfer in Rotating Cavity with a Peripheral Inflow and Outflow of Cooling Air" ASME Int. Gas Turbine Congress, ASME Paper No 97-GT-136, Orlando, 1997
9. Owen, J.M. and Rogers, R.H., "Flow and Heat Transfer in Rotating Disc Systems: Vol. 1, Rotor-stator systems", Research Studies Press, Taunton, UK and John Wiley, NY, 1989
10. Owen, J.M. and Wilson, M., "Some Current Research in Rotating-disc Systems", Turbine 2000 Int. Symp. on Heat Transfer in Gas Turbine Systems, August 13-18, in Heat Transfer in Gas Turbine Systems, Annals of the New York Academy of Sciences, Turkey, Vol 934, pp. 206-221, 2000
11. Lauder, B.E. and Sharma, B.L., "Applications of the Energy Dissipation Model of Turbulence to the Calculation of Flow Near a Spinning Disc", Letters in Heat and Mass Transfer, Vol. 1, pp. 131-138, 1974
12. Gosman, A.D. and Iferiah F.J.K., Tech-T, "A General Computer Program for Two Dimensional Turbulent Recirculating Flows in Calculations of Recirculating Flows", Mech. Eng. Dept., Imperial College, Univ. of London, 1976
13. Lock, G.D., Yan, Y., Newton, P.J., Wilson, M., and Owen, J. M., "Heat Transfer Measurements using Liquid Crystal in a Pre-swirl Rotating-disc System", ASME paper, GT-2003-38123, 2003
14. Pilbrow, R., Karabay, H., Wilson, M., and Owen, J.M., "Heat Transfer in a Cover-plate Pre-swirl Rotating-disc System", J. Turbomachinery, Vol. 121, No. 1, pp 249-256, 1999
15. Craft, T.J., Graham, L.J.W. and Launder, B.E. "Impinging Jet Studies for Turbulence Model Assessment-II., An Examination of the Performance of Four Turbulence Models". Int. J. Heat Mass Transfer, Vol. 36, No. 2, pp. 2685-2697, 1993

Table (1): The components of the transport equations.

ϕ	Γ_z	Γ_r	Γ_ϕ	S_ϕ
1	***0***	***0***	***0***	***0***
V_r	$2\mu_t+\mu$	$\mu_t+\mu$	$\mu_t+\mu$	$\frac{P}{r}+\frac{\rho V_\phi^{\,2}}{r}-\frac{2\mu_{eff}}{r^2}\frac{\partial V_\phi}{\partial\phi}-(2\mu_t+\mu)\frac{V_r}{r^2}-\frac{\partial(\rho k)}{\partial r}+\left(\mu_t\frac{\partial V_z}{\partial r}\right)+\mu_t\frac{\partial}{\partial\phi}\left(\frac{\partial}{\partial r}\left(\frac{V_\Phi}{r}\right)\right)+\underline{2\rho\Omega V_\phi}$
V_ϕ	$\mu_{t+}\mu$	$2\mu_t+\mu$	$\mu_t+\mu$	$\frac{1}{r}\frac{\partial}{\partial r}\left(\mu_t\frac{\partial V_r}{\partial\phi}\right)-\frac{V_\phi}{r}\frac{\partial\mu_t}{\partial r}+\frac{3\mu_t+2\mu}{r^2}\frac{\partial V_r}{\partial\phi}+\frac{2V_r}{r^2}\frac{\partial\mu_t}{\partial\phi}-\frac{1}{r}\frac{\partial}{\partial\phi}(P+\rho k)-\frac{\mu_{eff}V_\phi}{r^2}+\frac{1}{r}\frac{\partial}{\partial z}\left(\mu_t\frac{\partial V_z}{\partial\phi}\right)-\frac{\rho V_r V\phi}{r}-\underline{2\rho\Omega V_r}$
V_z	$2\mu_t+\mu$	$\mu_t+\mu$	$\mu_t+\mu$	$-\frac{\partial}{\partial z}(P+\rho k)+\frac{1}{r}\frac{\partial}{\partial r}\left(r\mu_t\frac{\partial V_r}{\partial z}\right)\frac{1}{r}\frac{\partial}{\partial\phi}\left(\mu_t\frac{\partial V_\phi}{\partial z}\right)$
T	$\frac{\mu}{\mathrm{Pr}}+\frac{\mu_t}{\mathrm{Pr}_t}$	$\frac{\mu}{\mathrm{Pr}}+\frac{\mu_t}{\mathrm{Pr}_t}$	$\frac{\mu}{\mathrm{Pr}}+\frac{\mu_t}{\mathrm{Pr}_t}$	$\frac{2\mu_{eff}}{c_p}\left[\left(\frac{\partial V_r}{\partial r}\right)^2+\left(\frac{\partial V_\phi}{r\partial\phi}+\frac{V_r}{r}\right)^2+\left(\frac{\partial V_z}{z}\right)^2\right]+\frac{2\mu_{eff}}{c_p}\left[r\frac{\partial}{\partial r}\left(\frac{V_\phi}{r}\right)+\frac{\partial V_r}{r\partial\phi}\right]^2+\frac{\mu_{eff}}{c_p}\left[\left(\frac{\partial V_z}{r\partial\phi}+\frac{\partial V_\phi}{\partial z}\right)^2+\left(\frac{\partial V_r}{\partial z}+\frac{\partial V_z}{\partial r}\right)^2\right]$
k	$\mu+\frac{\mu_t}{\sigma_k}$	$\mu+\frac{\mu_t}{\sigma_k}$	$\mu+\frac{\mu_t}{\sigma_k}$	$P_e-\rho\varepsilon-D$
ε	$\mu+\frac{\mu_t}{\sigma_\varepsilon}$	$\mu+\frac{\mu_t}{\sigma_\varepsilon}$	$\mu+\frac{\mu_t}{\sigma_\varepsilon}$	$\frac{\varepsilon}{k}(C_{\varepsilon1}P_e-C_{\varepsilon2}\rho\varepsilon)+E$

Table (2): Terms appearing in the turbulence model.

D	$2\mu\left[\left(\frac{\partial\sqrt{k}}{\partial z}\right)^2+\left(\frac{\partial\sqrt{k}}{\partial r}\right)^2+\left(\frac{\partial\sqrt{k}}{r\partial\phi}\right)^2\right]$
E	$2\frac{\mu\mu_t}{\rho}\left[\left(\frac{\partial^2 V_r}{\partial z^2}\right)^2+\left(\frac{\partial^2 V_\phi}{\partial z^2}\right)^2+\left(\frac{\partial^2 V_z}{\partial r^2}\right)^2+\left(\frac{\partial^2 V_\phi}{\partial r^2}\right)^2+\left(\frac{1}{r^2}\frac{\partial^2 V_r}{\partial\phi^2}\right)^2+\left(\frac{1}{r^2}\frac{\partial^2 V_z}{\partial\phi^2}\right)^2\right]$
F	***0***
f_1	$1-0.3\exp\left(-R_t^2\right)$
f_μ	$\exp\left[\frac{-3.4}{\left(1+\frac{R_t}{50}\right)^2}\right]$
σ_k	***1***
σ_e	***1.3***